CrossMark

ARTICLE

Investigation of Single-Wall MoS₂ Monolayer Flakes Grown by Chemical Vapor Deposition

Nihan Kosku Perkgoz[1] · Mehmet Bay[1]

Abstract Recently, two-dimensional monolayer molybdenum disulfide (MoS₂), a transition metal dichalcogenide, has received considerable attention due to its direct bandgap, which does not exist in its bulk form, enabling applications in optoelectronics and also thanks to its enhanced catalytic activity which allows it to be used for energy harvesting. However, growth of controllable and high-quality monolayers is still a matter of research and the parameters determining growth mechanism are not completely clear. In this work, chemical vapor deposition is utilized to grow monolayer MoS₂ flakes while deposition duration and temperature effect have been systematically varied to develop a better understanding of the MoS₂ film formation and the influence of these parameters on the quality of the monolayer flakes. Different from previous studies, SEM results show that single-layer MoS₂ flakes do not necessarily grow flat on the surface, but rather they can stay erect and inclined at different angles on the surface, indicating possible gas-phase reactions allowing for monolayer film formation. We have also revealed that process duration influences the amount of MoO₃/MoO₂ within the film network. The homogeneity and the number of layers depend on the change in the desorption–adsorption of radicals together with sulfurization rates, and, inasmuch, a careful optimization of parameters is crucial. Therefore, distinct from the general trend of MoS₂ monolayer formation, our films are rough and heterogeneous with monolayer MoS₂ nanowalls. Despite this roughness and the heterogeneity, we observe a strong photoluminescence located around 675 nm.

Keywords Monolayer · Chemical vapor deposition · Two-dimensional materials · Molybdenum disulfide (MoS₂)

1 Introduction

As the dimensions of materials are reduced from three dimensions (3D), the fundamental physical properties change remarkably, allowing for novel applications, which are otherwise not possible [1, 2]. Transition from 3D to two dimensions (2D) first became possible with the exfoliation of graphene, a material well-known for its high electron mobility, mechanical strength, and thermal conductivity [3–6]. Unfortunately, there are still important challenges involved in the transition of graphene from laboratories to industry especially due to its zero bandgap [7]. Therefore, researchers are still in search of a novel material system preferably with a direct bandgap to be used in electronic, photonic, and energy applications. In this regard, transition metal dichalcogenides (TMDC), MX₂ (M = Mo, W; X = S, Se, Te) are receiving special attention with their peculiar optical and electronic properties [8–10] and their potential to be used in catalysis, microelectronics, batteries, hydrogen storage, medical applications, and optoelectronics [11–14]. Among the numerous candidates, monolayer MoS₂ has invoked a particular interest due to its direct bandgap and it is considered to have great potential both in electronics and photonics [15–17]. MoS₂-based field effect transistors (FETs) used as phototransistors, memory devices, and sensors have shown superior properties including excellent mobility, ON/OFF ratio, and sensitivity [18].

✉ Nihan Kosku Perkgoz
nkperkgoz@anadolu.edu.tr

1 Department of Electrical and Electronics Engineering, Faculty of Engineering, Anadolu University, 26555 Eskisehir, TR, Turkey

Also, MoS_2 has attracted attention due to its thermal properties and its potential use in thermoelectric applications [18, 19] and catalyzing properties resulting from its active edge sites [20]. However, scalable, controllable, large-area growth of single-layer MoS_2, keeping high crystal quality and large domain size, still remains a problem [14, 21]. Mechanical exfoliation, one of the most commonly used methods, is not favorable for commercial applications. Likewise, liquid exfoliation, ionic intercalation, and hydro-thermal methods still have important drawbacks where batch fabrication and device applications are concerned [22–25]. It is also possible to form different few-layer TMDCs through colloidal synthesis techniques, which are beneficial in terms of high-yield and substrate-free nanostructures [26]. However, developing a facile and reliable method for large-area growth is crucial in order to use such 2D materials in the different applications of electronics and photonics.

One method which seems particularly promising is chemical vapor deposition (CVD), as it is highly promising in its ability to grow monolayer, controlled, large-area MoS_2 films [14, 21, 27–29]. CVD-based synthesis was first reported in 2012 [21, 22], showing the potential of the method to realize high-quality, controlled growth of the MoS_2 flakes, and other researches have revealed that monolayer flakes deposited by CVD can be used in different applications and devices such as phototransistors [30], photodetectors [31], memories [16], and so on. Although the underlying mechanism of the monolayer MoS_2 growth is still not very clear, it can allow for determining the features of the thin films through controlled synthesis [32–34].

In the present work, we have used CVD to obtain single-wall monolayer MoS_2 flakes whose features can be changed through process parameters. We report the direct influence of deposition duration and process temperature on the growth mechanism and film properties. By changing process parameters, we can shift from a rough surface with MoS_2 flakes scattered at different angles to a smoother and more uniform surface composed of monolayer MoS_2 formations. Such single-wall MoS_2 flakes, which for the most part are not flat on the surface, can be beneficial in applications including solar cells [35], energy storage [36], catalysis [11], and sensing [37] where large surface area of the flakes can increase the intended performance.

2 Experimental

The experimental setup of the CVD system is schematically shown in Fig. 1. The quartz boats containing high-purity MoO_3 (14 mg, 99.9 %, Aldrich) and S powder (1.4 g, 99.5 %, Alfa) were placed at the temperature zones specified according to the melting temperatures of the precursors, 700 °C for MoO_3 and 150 °C for sulfur. The MoO_3 boat was located at the highest temperature zone of the furnace. In our setup, spatial locations have been critical for complete sulfurization and monolayer MoS_2 formation as the temperature changes with distance. This effect was investigated by varying the distance between boats of MoO_3 powder and the substrates (D_s) from 9 cm ($\sim$670 °C) to 13 cm ($\sim$600 °C). The SiO_2 ($\sim$300 nm)-coated Si substrates are cleaned using piranha etch solution and the RCA technique. SiO_2 was thermally grown on Si, and the thickness is confirmed by ellipsometry. Before deposition started, the reaction chamber was heated to deposition temperature at a rate of 15 °C min^{-1} in a nitrogen environment, and at the specified deposition temperatures, Ar and H_2 were introduced to the system as carrying gases at flow rates of 17 and 10 sccm, respectively. The growth duration was decreased from 10 to 5 and 3 min to observe the evolution of the flakes.

At deposition temperatures, S vapor reduced MoO_3 powder to volatile suboxide MoO_{3-x} [38] and MoS_2 monolayer flakes were formed by the gas-phase reactions while the compounds diffusing on the substrate reacting with sulfur are obtained possibly through the Eqs. (1) and (2) [21]. It is suggested that if the reaction duration is not sufficient, the sulfurization process cannot be fully accomplished and intermediate products are formed, one of which is MoO_2, due to its stability [38]. After the growth period was finished, a rapid cooling-down process was carried out and 500 sccm of nitrogen gas (99.999 %) was purged into the tube to avoid other products such as MoO_3 formation while keeping MoS_2 monolayers on the surface of the substrate.

$$MoO_3 + (x/2)S \rightarrow MoO_{3-x} + (x/2)SO_2, \tag{1}$$

$$MoO_{3-x} + (7-X)/2\ S \rightarrow MoS_2 + (3-X)/2\ SO_2. \tag{2}$$
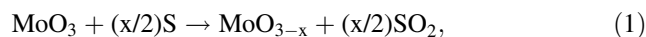
The MoS_2 monolayer formations were characterized by Raman spectroscopy, photoluminescence (PL), scanning electron microscopy (SEM), and high-resolution transmission electron microscopy (HRTEM). In the case of MoS_2 deposition, Raman spectroscopy is a practical and facile way to examine the film properties including the number of layers and the imprints of other possible products such as MoO_3, MoO_{3-x}, and MoO_2 [39–42]. In bulk MoS_2, there are two distinctive Raman peaks corresponding to in-plane vibration of Mo and S atoms (E_{2g}^1) at $\sim$383 cm^{-1} and the out-of-plane vibration of S atoms (A_{1g}) at $\sim$408 cm^{-1} where the number of layers are determined by the change in difference between these two peaks [41]. As the number of layers decrease, the mode at E_{2g}^1 is found to move to lower frequencies and the mode at A_{1g} is found to move to higher frequencies [22, 39], giving valuable information
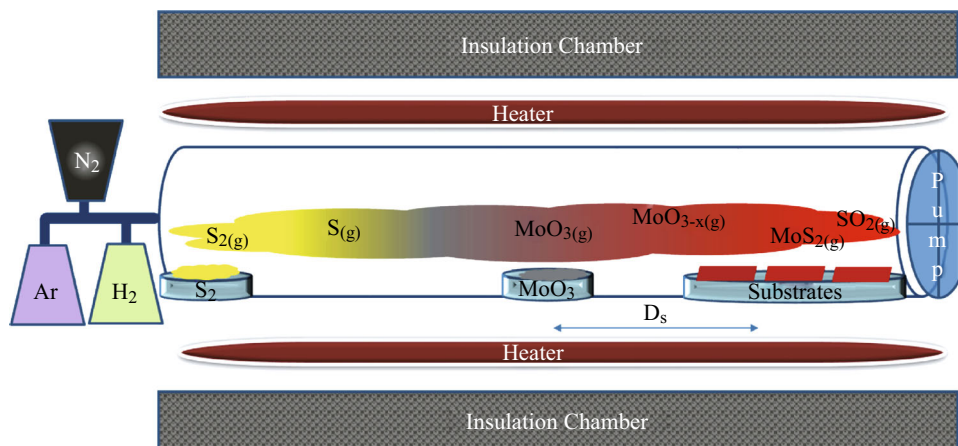
72

Nano-Micro Lett. (2016) 8(1):70–79

Fig. 1 The chemical vapor deposition system for the deposition of MoS_2 flakes

about monolayer and multi-layer MoS_2 flakes. Additionally, these peaks also shift with the change in film properties, the frequency of E^1_{2g} vibrational mode is found to be effected by strain [43], and the frequency of A_{1g} vibrational mode is found to depend on electrostatic doping [44]. PL also gives valuable information about the transition from bulk or multi-layer indirect-bandgap MoS_2 to direct-bandgap, few-layer or monolayer MoS_2 flakes. For the PL measurements, a focused excitation laser (532 nm) was used to detect the peaks at ~ 670 nm (A_1 excitation of MoS_2) and ~ 630 nm (the resonance of B_1 excitation) for MoS_2 films [45]. At about 645 nm, a peak which is the sign of bilayer MoS_2 can also be observed [46]. While the peak at ~ 630 nm is related with rather thick flakes as the layers go from multi-layer to monolayer MoS_2, the peak around 670 nm gets more intense and sharper [47]. In addition to number of layers, photoluminescence also depends on various parameters including grain sizes, defects, strain, and electrostatic doping [27, 32].

SEM was utilized to investigate the shapes of the flakes and see the general view of the film formations. HRTEM was used a supportive technique for further understanding about the shapes of the flakes. In addition to this analysis, investigation of defect states and vacancies is important as they affect the transport mechanism and PL of the system [48–51]. However, in this research work, we rather focused on the properties of the nanowall film formations and their dependence on the process parameters.

3 Results and Discussion

MoS_2 flakes have been grown using solid MoO_3 and S as precursors at different spatial locations, abbreviated as D_s (distance between MoO_3 powder boat and the substrates) as illustrated in Fig. 1. As shown in Fig. 2a, b, Raman

scattering (excitation wavelength at 532 nm) and PL spectra are primarily analyzed to identify the film characteristics including the number of MoS_2 layers and formation of other products different from MoS_2 [52, 53]. In the first set of experiments, D_s is changed from 10 to 13 cm while the deposition time is fixed to 10 min. The change in the distance can be indicative of the change in precursor concentration [34]. However, with our setup (Fig. 1), this effect can be ignored where the substrate temperature (T_S) changing with the distance is suggested to be a rather more effective parameter to influence the film properties.

As presented in Fig. 2a, although the two distinctive MoS_2 Raman peaks (around ~ 379 and ~ 402 cm^{-1} corresponding to in-plane vibration of Mo and S atoms according to the Raman peaks) are present, we also observe Raman signatures from oxide phases (MoO_3 and/or MoO_x) which indicate the presence of residual oxygen associated with incomplete sulfurization. The peak at ~ 299 cm^{-1} is an indicator of nanometer-thick MoO_3 sheets (as small as ~ 15 nm), and it can be correlated with the stoichiometry of MoO_3 polycrystalline samples or a shift of an initially strong 284 cm^{-1} peak [54, 55]. At $D_S = 10$ cm, a small peak located at 231 cm^{-1} is observed, most probably due to one-dimensional MoO_2 nanorods [45], and at $D_S = 11$ cm, another weak peak centered around 198 cm^{-1} is explained by the formation of thick MoO_3 sheets (~ 300 nm) [54]. As the distance (D_s) becomes larger than 12 cm, the peak at 246 cm^{-1} starts to be more visible, indicative of B^3_g twist mode, showing that the MoO_3 nanoparticles get larger at lower substrate temperatures [54]. We can suggest that when the temperature is not sufficiently high, the activation energy of the reactions in Eq. (2) is not provided. In fact, from the Raman peaks, measured from the films formed at a distance of 10 cm (T_S of ~ 655 °C), the imprints of MoO_3 nanoparticles are also observed. In this case, it is quite probable that the diffusion
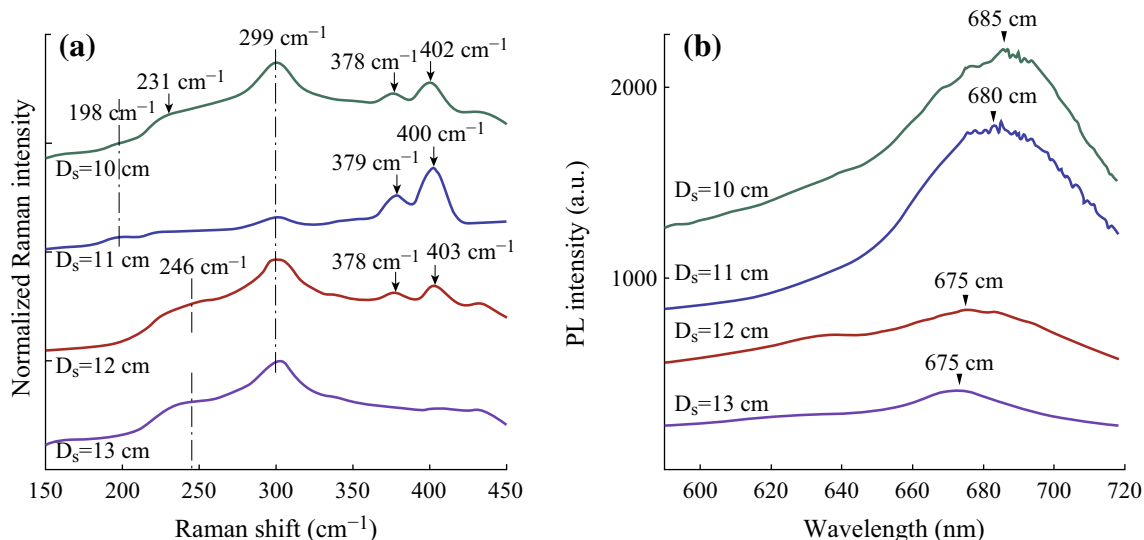
Fig. 2 **a** Raman scattering and **b** PL spectra of the films grown on SiO_2 coated Si substrate for D_s values between 10 and 13 cm while the reaction period is fixed to 10 min

of the sulfur species is degraded and formation of MoO_3 nanoparticles is more likely than the formation of MoS_2 flakes. These results show that balancing desorption–adsorption and sulfurization rates is crucial to obtain high-quality, monolayer MoS_2 flakes. Obviously, the network that we obtained is not homogeneous, and there are different MoO_x ($X = 2, 3$) sheets and rods being formed during the deposition, which also helps the MoS_2 flakes to be suspended on the surface allowing for a larger surface area.

MoO_3 and/or MoO_x peaks are ignorable only for the sample deposited at $D_s = 11$ cm (T_S of ~655 °C), which suggests that the deposited MoS_2 flakes are rather uniform and high quality with an optimized substrate temperature of precursor ratio of MoO_3 to S. This can be explained by the efficient adsorption and diffusion of MoO_{3-x} species on the substrate and reaction with S to form MoS_2 at around 640 °C. Although other substrate temperature regimes also have been reported for MoS_2 formation [14, 33], it is concluded that due to the complicated nucleation process, it is possible to find different optimal conditions to grow monolayer MoS_2 flakes in different systems. Therefore, depending on the system geometry, flow rates, and other process parameters, the substrate temperature should be carefully controlled to fine-tune the adsorption/desorption of radicals and the sulfurization rate for the growth of MoS_2 monolayers [56]. Our results show that the difference in Raman peaks is between 21 and 25 cm^{-1} corresponding to in-plane vibration of Mo and S atoms (E_{2g}^1) at ~378–379 cm^{-1} and the out-of-plane vibration of S atoms (A_{1g}) at ~400–403 cm^{-1}. Both E_{2g}^1 and A_{1g} modes exhibit a blueshift when compared to bulk MoS_2 in agreement with

other nanowall-like MoS_2 layers [57]. However, the peak convergence is less than that of the reported monolayer MoS_2 results in the literature, which can be explained by the fact that the network is not completely composed of monolayer MoS_2 formations, but the film, specifically the parts closer to the substrate surface, contains oxysulfides ($MoOS_2$), MoO_x ($X = 2, 3$), and multi-layer flakes [51, 58, 59]. High-temperature conditions ($D_s = 10$ cm) are considered unfavorable for MoS_2 monolayer formation due to their high diffusion rate, which obstructs the growth of stable nuclei.

As shown in Fig. 2b, although their full width at half maximum (FWHM) is not narrow, the PL peaks between ~675 and ~685 nm indicate formation of monolayer MoS_2 flakes, specifically at a distance (D_s) of 11 cm. At this specified spatial location, more homogeneous and rather large-size MoS_2 mono layers are formed and a stronger photoluminescence develops, which results from the direct excitonic transition due to the direct bandgap of monolayer MoS_2 [47]. For the films deposited at other substrate temperatures, the intensity of peaks becomes lower and their FWHM becomes wider. In general, the formed structures are not uniform, and, especially at low temperatures, the roughness and heterogeneity increase.

Figure 3 exhibits the SEM pictures of the films in Fig. 2, giving information about the size, shape of the flakes, and general network of the formations. These images show features similar to nanowalls and nano-plates that are edge oriented due the basal edges deposited on the substrate [60]. Such nanowall-like structures are appealing for their potential to be used as super capacitors, specifically in Li-ion batteries [36, 61–63]. Also, high surface area can be
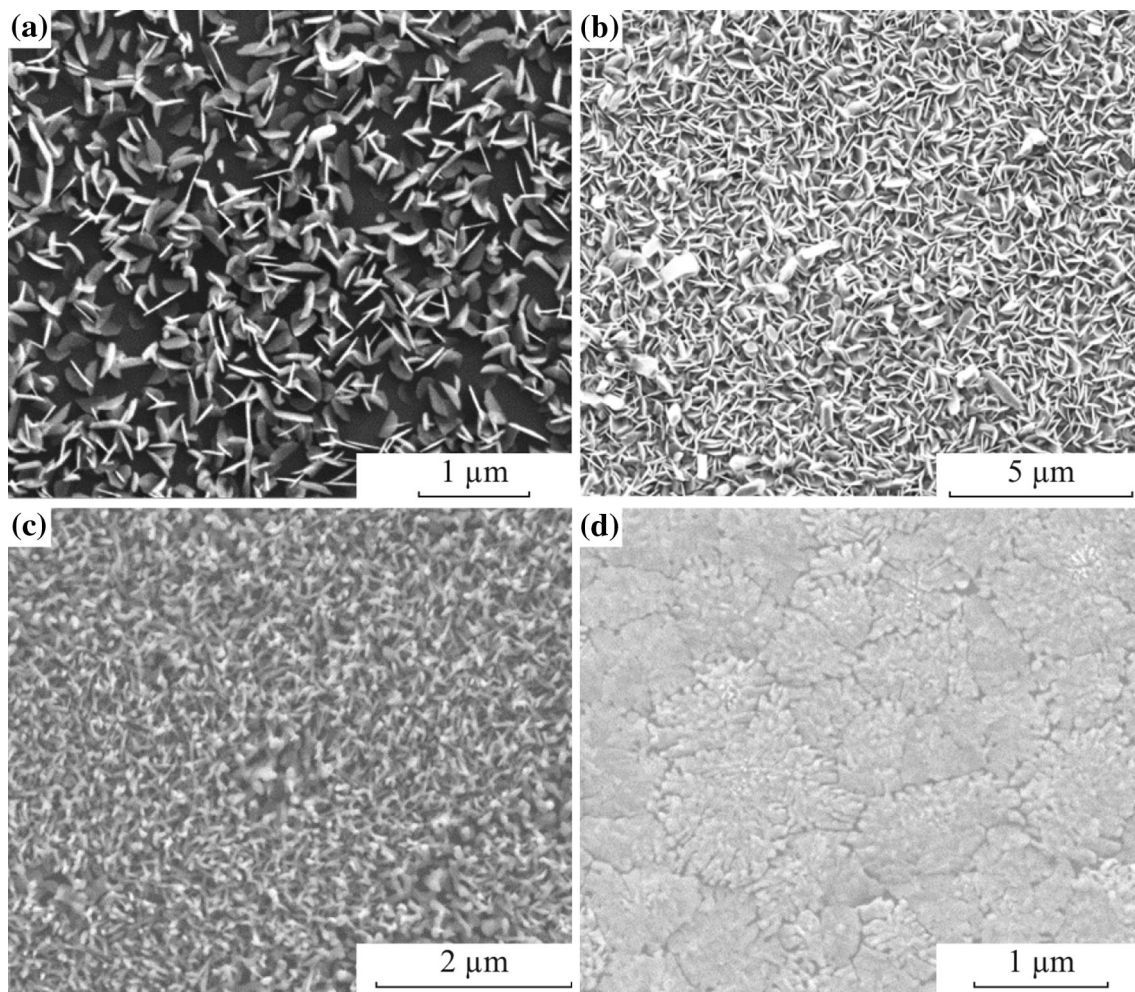
Fig. 3 SEM Images for the films deposited when D_s = **a** 10 cm, **b** 11 cm, **c** 12 cm, and **d** 13 cm with a reaction period of 10 min

beneficial when used in heterostructures where non-radiative energy transfer is utilized. Rather high crystal growth rate and large number of nucleation sites are considered to provide smaller crystalline grain sizes. As a result, the formed surface is not homogeneous and the surface is far from being smooth. When the substrate temperature is reduced (at D_s = 13 cm), the surface roughness decreases and such nanowall-like structures become less visible (Fig. 3d).

It is expected that process duration and the concentration of the reactants also play a crucial role in the formation of MoS_2 films. Therefore, to get a better understanding of the growth mechanism, we decreased the deposition duration from 10 to 5 min. Figure 4a, b shows Raman scattering and PL spectra, respectively. Indeed, both the Raman scattering and PL spectra exhibit that a more homogeneous network is obtained along with a much reduced amount of other types of formations such as $MoOS_2$, MoO_2, or MoO_3. The peak at ~ 299 cm^{-1}, an indicator of nanometer-thick MoO_3 sheets. has nearly disappeared, and the difference in

MoS_2 Raman peak has become as small as ~ 22 cm^{-1}. This Raman peak difference, higher than expected, could be explained with a large number of small-size grains or crystalline defects. Different from the Raman scattering spectra measured from the films deposited in 10 min, another peak at ~ 355 cm^{-1} starts to develop, indicative of m-MoO_2 b-MoO_{3-x} phase transition [64]. This suggests that in 5 min, S vapor has reduced MoO_3 powder to volatile suboxide MoO_{3-x} [32] and in 10 min, these MoO_{3-x} regions have already been transformed into either MoS_2 monolayer flakes or MoO_3 nanoparticles (see Fig. 2a). As the substrate distances get larger, a peak around 365 cm^{-1}, assigned to O–Mo–O bending and scissoring modes, also becomes more visible [65].

It should be noted that there is also a significant improvement in the PL characteristics of the films deposited in 5 min (Fig. 4b) compared to the films with a reaction period of 10 min (Fig. 2b). This improvement is observed specifically for the films that are deposited at a D_S of 11 cm (T_S of ~ 640 °C). MoS_2 flakes are mostly in the
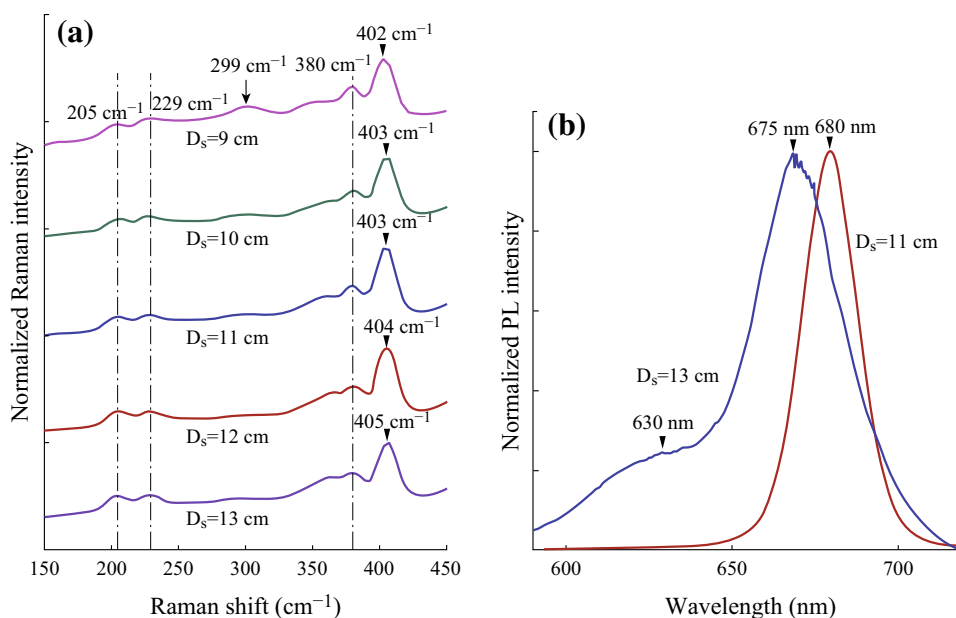
Fig. 4 **a** Raman scattering spectra for films deposited at D_S values between 9 and 13 cm; **b** PL spectra for the films deposited at $D_S = 11$ and 13 cm while the reaction period is fixed to 5 min

form of single layers, which is understood from the disappearing peak at ~ 630 nm, an indicator of multi-layer flakes. Also, the peak at ~ 675 shifts to ~ 680 nm and becomes narrower, showing higher-quality and homogeneous flakes at a D_s of 11 cm compared to the case at a D_s of 13 cm. The PL spectra at 9, 10, and 12 cm are not included in the Figure because they do not show a significant difference from the peak obtained from the film deposited at the D_S of 13 cm. In general, these results explain that sulfurization in the first 5 min is sufficient; however, as the deposition period is increased, other products start to develop. It is obvious that optimizing the precursor concentrations is also crucial to prevent molybdenum di/three oxide sheets and allows for the formation of large MoS$_2$ monolayers, and these parameters are specific to the experimental setup and deposition temperature. As described by Wang et al., edge free energy and the ratio (or amount) of the precursors in the medium are the determining factors for the growing rate and hence the shape of the grains [34].

Figure 5 presents the SEM images of these films formed in 5 min. Different from the films formed in 10 min, the flakes are visible specifically when deposited at a D_s of 9, 10, and 11 cm. Commonly, it is discussed that the domain shape of the flakes tend to grow in the form of a triangle or a hexagon [34]. However, most of our MoS$_2$ flakes are in the shape of half pringles resembling truncated triangles where the shapes of domains are suggested to be controlled by the ratio of precursors effecting the kinetic growth dynamics of edges [27, 58].

SEM images also show that flakes are not flat on the surface of the substrate but rather they appear to stand erect with different angles. These observations confirm that gas-phase reactions are effective in our system making MoS$_2$ flakes round-shaped and erect on the surface instead of being flat on the surface.

Observing the improvement in the formation of MoS$_2$ monolayers with a decreased deposition duration of 5 min with respect to the case of 10 min, this period is further reduced to 3 min. Figure 6a shows Raman scattering spectra of the films formed in 3, 5, and 10 min when D_s is fixed to 11 cm. Interestingly, the peak at ~ 299 cm^{-1} has again become visible, showing that nanometer-thick MoO$_3$ sheets are formed on the surface. This result is due to insufficient deposition duration for MoS$_2$ flakes to form. Figure 6b confirms that the flakes are relatively small when compared with the ones in Fig. 5.

We investigated selected-area electron diffraction and HRTEM (FEI TECNAI G2 F30 model) images with an accelerating voltage of 200 kV to have further understanding of flake structures. The HRTEM image in Fig. 7a, b exhibits a monolayer MoS$_2$ triangular and "chips-like" shape where Fig. 7c shows the periodic atomic arrangement. As it can be observed from the SEM images (Figs. 3, 5), most of the flakes are "chip-like" in shape, and triangular-shaped flakes also exist in the film network. Figure 7d displays diffraction patterns of a monolayer triangular flake. These single flakes have been prepared using the as-grown films through simply rinsing in water and drop casting the solution on a TEM grid. The
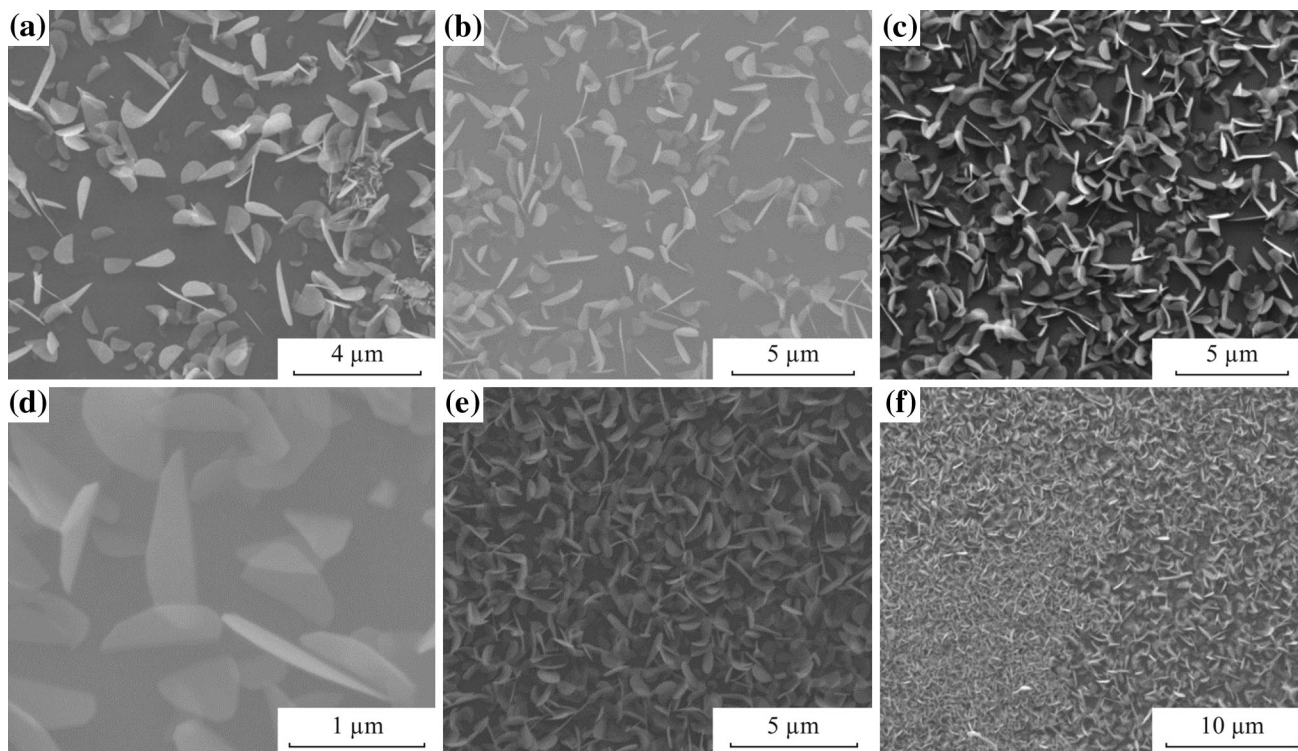
Fig. 5 SEM Images for CVD MoS$_2$ on SiO$_2$-coated Si substrate when D_s = **a** 9 cm, **b** 10 cm, **c**, **d** 11 cm, **e** 12 cm, and **f** 13 cm with a reaction period of 5 min
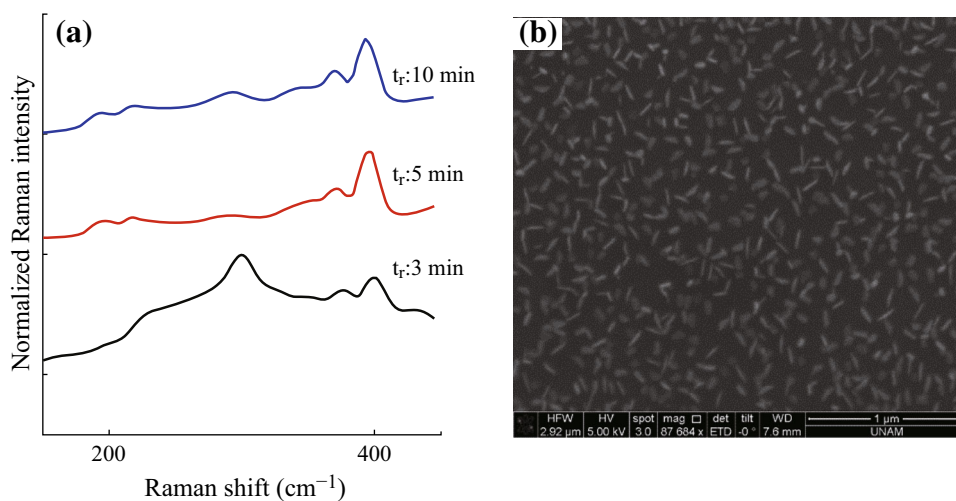

Fig. 6 a Raman spectra for CVD MoS$_2$ on SiO$_2$-coated Si substrate when the reaction period is fixed to 3, 5, and 10 min when D_S is fixed to 11 cm; **b** SEM image with a reaction period of 3 min

symmetry in the diffraction spots show that the flake is a continuous single crystal, and there are no rotational boundaries. Corresponding selective area electron diffraction (SAED) pattern with [001] zone axis shows hexagonally arranged diffraction spots assigned to the (100) and (110) planes [21] suggestive of the highly crystalline nature of the MoS$_2$ flakes.

4 Conclusions

We have shown that when substrate temperature and growth duration are controlled, MoS$_2$ flakes with different properties including nanowall-like rough surfaces and relatively smoother monolayer MoS$_2$ surfaces can be grown. Also, side products such as MoO$_3$ and MoO$_2$ can be
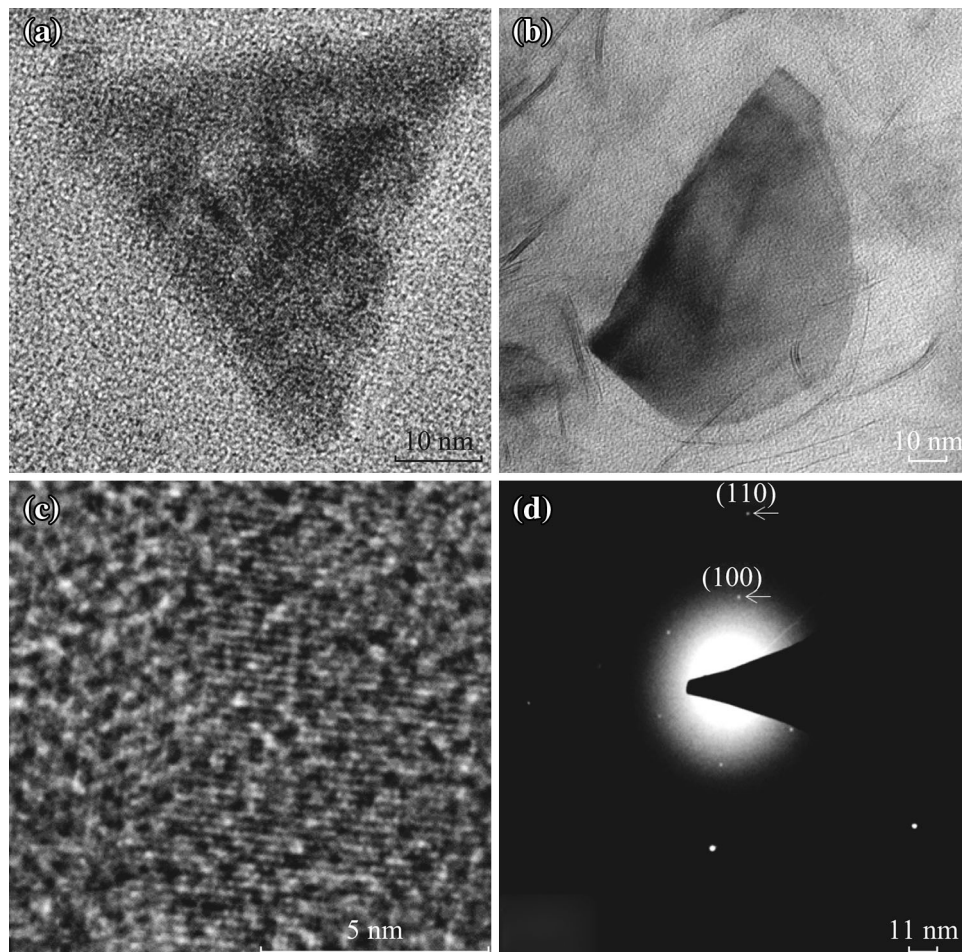
Fig. 7 TEM Image of **a** triangular and **b** chips-like shapes **c** periodic atomic arrangement, **d** diffraction patterns of a monolayer triangular flake

avoided by fine-tuning the process parameters. Due to the complicated nucleation and growth process, it is important to optimize these parameters in different system geometries and flow rates to adjust the adsorption/desorption of radicals obtain sufficient sulfurization rates and find optimal conditions to grow monolayer MoS_2 flakes. In our experiments, in addition to triangular flakes, we obtained rounded flakes resembling truncated triangles, which are not flat on the surface but rather erect at different angles. This result suggests that gas-phase reactions are also effective in monolayer MoS_2 formation. Despite the roughness and heterogeneity of the formed network, we obtained films exhibiting a strong PL peak, a characteristic behavior of monolayer flakes, due the erect monolayer MoS_2 nanowalls. These results show that such single-wall MoS_2 flakes, which are mostly not flat on the surface, possess a rather larger surface area and can be beneficial in applications such as solar cells, energy storage, catalysis, and sensors with higher performance.

References

1. F.N. Xia, H.G. Yan, P. Avouris, The interaction of light and graphene: basics, devices, and applications. Proc. IEEE **101**(7), 1717–1731 (2013). doi:10.1109/JPROC.2013.2250892
2. Y. Zhu, S. Murali, W. Cai, X. Li, J.W. Suk, J.R. Potts, R.S. Ruoff, Graphene and graphene oxide: synthesis, properties, and applications. Adv. Mater. **22**(35), 3906–3924 (2010). doi:10.1002/adma.201001068
3. A.K. Geim, Graphene: status and prospects. Science **324**(5934), 1530–1534 (2009). doi:10.1126/science.1158877
4. F. Bonaccorso, Z. Sun, T. Hasan, A.C. Ferrari, Graphene photonics and optoelectronics. Nat. Photonics **4**(9), 611–622 (2010). doi:10.1038/nphoton.2010.186

5. E. Pop, V. Varshney, A.K. Roy, Thermal properties of graphene: fundamentals and applications. MRS Bull. **37**(12), 1273–1281 (2012). doi:10.1557/mrs.2012.203

6. Z. Yang, R. Gao, N. Hu, J. Chai, Y. Cheng, L. Zhang, H. Wei, E.S.-W. Kong, Y. Zhang, The Prospective 2D graphene nanosheets: preparation functionalization and applications. Nano-Micro Lett. **4**(1), 1–9 (2011). doi:10.3786/nml.v4i1.p1-9

7. F. Xia, D.B. Farmer, Y.-M. Lin, P. Avouris, Graphene field-effect transistors with high on/off current ratio and large transport band gap at room temperature. Nano Lett. **10**(2), 715–718 (2010). doi:10.1021/nl9039636

8. Q. Xiang, J. Yu, M. Jaroniec, Synergetic effect of MoS_2 and graphene as cocatalysts for enhanced photocatalytic H_2 production activity of TiO_2 nanoparticles. JACS **134**(15), 6575–6578 (2012). doi:10.1021/ja302846n

9. H.-P. Komsa, A.V. Krasheninnikov, Two-dimensional transition metal dichalcogenide alloys: stability and electronic properties. J. Phys. Chem. Lett. **3**(23), 3652–3656 (2012). doi:10.1021/jz301673x

10. T.C. Berkelbach, M.S. Hybertsen, D.R. Reichman, Theory of neutral and charged excitons in monolayer transition metal dichalcogenides. Phys. Rev. B **88**(4), 045318 (2013). doi:10.1103/PhysRevB.88.045318

11. Y. Li, H. Wang, L. Xie, Y. Liang, G. Hong, H. Dai, MoS_2 nanoparticles grown on graphene: an advanced catalyst for the hydrogen evolution reaction. JACS **133**(19), 7296–7299 (2011). doi:10.1021/ja201269b

12. K. Chang, W. Chen, L-cysteine-assisted synthesis of layered MoS_2/graphene composites with excellent electrochemical performances for lithium ion batteries. ACS Nano **5**(6), 4720–4728 (2011). doi:10.1021/nn200659w

13. Q. Ji, Y. Zhang, T. Gao, Y. Zhang, D. Ma et al., Epitaxial monolayer MoS_2 on mica with novel photoluminescence. Nano Lett. **13**(8), 3870–3877 (2013). doi:10.1021/nl401938t

14. J. Shi, D. Ma, G.-F. Han, Y. Zhang, Q. Ji, T. Gao, J. Sun, X. Song, C. Li, Y. Zhang, Controllable growth and transfer of monolayer MoS_2 on Au foils and its potential application in hydrogen evolution reaction. ACS Nano **8**(10), 10196–10204 (2014). doi:10.1021/nn503211t

15. A. Splendiani, L. Sun, Y.B. Zhang, T.S. Li, J. Kim, C.Y. Chim, G. Galli, F. Wang, Emerging photoluminescence in monolayer MoS_2. Nano Lett. **10**(4), 1271–1275 (2010). doi:10.1021/nl903868w

16. X. Tong, E. Ashalley, F. Lin, H. Li, Z.M. Wang, Advances in MoS_2-based field effect transistors (FETs). Nano-Micro Lett. **7**(3), 203–218 (2015). doi:10.1007/s40820-015-0034-8

17. F. Prins, A.J. Goodman, W.A. Tisdale, Reduced dielectric screening and enhanced energy transfer in single-and few-layer MoS_2. Nano Lett. **14**(11), 6087–6091 (2014). doi:10.1021/nl5019386

18. C. Sevik, Assessment on lattice thermal properties of two-dimensional honeycomb structures: graphene, h-BN, h-MoS_2, and h-$MoSe_2$. Phys. Rev. B **89**(3), 035422 (2014). doi:10.1103/PhysRevB.89.035422

19. W. Huang, X. Luo, C.K. Gan, S.Y. Quek, G. Liang, Theoretical study of thermoelectric properties of few-layer MoS_2 and WSe_2. Phys. Chem. Chem. Phys. **16**(22), 10866–10874 (2014). doi:10.1039/c4cp00487f

20. Z. Zhou, Y. Lin, P. Zhang, E. Ashalley, M. Shafa, H. Li, J. Wu, Z. Wang, Hydrothermal fabrication of porous MoS_2 and its visible light photocatalytic properties. Mater. Lett. **131**, 122–124 (2014). doi:10.1016/j.matlet.2014.05.162

21. Y.-H. Lee, X.-Q. Zhang, W. Zhang, M.-T. Chang, C.-T. Lin et al., Synthesis of large-area MoS_2 atomic layers with chemical vapor deposition. Adv. Mater. **24**(17), 2320–2325 (2012). doi:10.1002/adma.201104798

22. Y. Zhan, Z. Liu, S. Najmaei, P.M. Ajayan, J. Lou, Large-area vapor-phase growth and characterization of MoS_2 atomic layers on a SiO_2 substrate. Small **8**(7), 966–971 (2012). doi:10.1002/smll.201102654

23. S. Wu, C. Huang, G. Aivazian, J.S. Ross, D.H. Cobden, X. Xu, Vapor-solid growth of high optical quality MoS_2 monolayers with near-unity valley polarization. ACS Nano **7**(3), 2768–2772 (2013). doi:10.1021/nn4002038

24. S. Balendhran, J.Z. Ou, M. Bhaskaran, S. Sriram, S. Ippolito et al., Atomically thin layers of MoS_2 via a two step thermal evaporation–exfoliation method. Nanoscale **4**(2), 461–466 (2012). doi:10.1039/C1NR10803D

25. J.N. Coleman, M. Lotya, A. O'Neill, S.D. Bergin, P.J. King, U. Khan, K. Young, A. Gaucher, S. De, R.J. Smith, Two-dimensional nanosheets produced by liquid exfoliation of layered materials. Science **331**(6017), 568–571 (2011). doi:10.1126/science.1194975

26. D. Sun, S. Feng, M. Terrones, R.E. Schaak, Formation and interlayer decoupling of colloidal $MoSe_2$ nanoflowers. Chem. Mater. **27**(8), 3167–3175 (2015). doi:10.1021/acs.chemmater.5b01129

27. A.M. van der Zande, P.Y. Huang, D.A. Chenet, T.C. Berkelbach, Y. You et al., Grains and grain boundaries in highly crystalline monolayer molybdenum disulphide. Nat. Mater. **12**(6), 554–561 (2013). doi:10.1038/nmat3633

28. K.-K. Liu, W. Zhang, Y.-H. Lee, Y.-C. Lin, M.-T. Chang et al., Growth of large-area and highly crystalline MoS_2 thin layers on insulating substrates. Nano Lett. **12**(3), 1538–1544 (2012). doi:10.1021/nl2043612

29. Y. Shi, W. Zhou, A.-Y. Lu, W. Fang, Y.-H. Lee et al., Van der waals epitaxy of MoS_2 layers using graphene as growth templates. Nano Lett. **12**(6), 2784–2791 (2012). doi:10.1021/nl204562j

30. W. Zhang, J.K. Huang, C.H. Chen, Y.H. Chang, Y.J. Cheng, L.J. Li, High-gain phototransistors based on a CVD MoS_2 monolayer. Adv. Mater. **25**(25), 3456–3461 (2013). doi:10.1002/adma.201301244

31. W. Zhang, C.-P. Chuu, J.-K. Huang, C.-H. Chen, M.-L. Tsai et al., Ultrahigh-gain photodetectors based on atomically thin graphene-MoS_2 heterostructures. Sci. Rep. **4**, 3826 (2014). doi:10.1038/srep03826

32. I.S. Kim, V.K. Sangwan, D. Jariwala, J.D. Wood, S. Park et al., Influence of stoichiometry on the optical and electrical properties of chemical vapor deposition derived MoS_2. ACS Nano **8**(10), 10551–10558 (2014). doi:10.1021/nn503988x

33. J. Zhang, H. Yu, W. Chen, X. Tian, D. Liu et al., Scalable growth of high-quality polycrystalline MoS_2 monolayers on SiO_2 with tunable grain sizes. ACS Nano **8**(6), 6024–6030 (2014). doi:10.1021/nn5020819

34. S. Wang, Y. Rong, Y. Fan, M. Pacios, H. Bhaskaran, K. He, J.H. Warner, Shape evolution of monolayer MoS_2 crystals grown by chemical vapor deposition. Chem. Mater. **26**(22), 6371–6379 (2014). doi:10.1021/cm5025662

35. M.-L. Tsai, S.-H. Su, J.-K. Chang, D.-S. Tsai, C.-H. Chen, C.-I. Wu, L.-J. Li, L.-J. Chen, J.-H. He, Monolayer MoS_2 heterojunction solar cells. ACS Nano **8**(8), 8317–8322 (2014). doi:10.1021/nn502776h

36. H. Hwang, H. Kim, J. Cho, MoS_2 nanoplates consisting of disordered graphene-like layers for high rate lithium battery anode materials. Nano Lett. **11**(11), 4826–4830 (2011). doi:10.1021/nl202675f

37. H. Li, Z. Yin, Q. He, H. Li, X. Huang, G. Lu, D.W.H. Fam, A.I.Y. Tok, Q. Zhang, H. Zhang, Fabrication of single- and multilayer MoS_2 film-based field-effect transistors for sensing no at room temperature. Small **8**(1), 63–67 (2012). doi:10.1002/smll.201101016

38. X.L. Li, Y.D. Li, Formation of MoS_2 inorganic fullerenes (IFs) by the reaction of MoO_3 nanobelts and S. Chem. Eur. J. **9**(12), 2726–2731 (2003). doi:10.1002/chem.200204635

39. C. Lee, H. Yan, L.E. Brus, T.F. Heinz, J. Hone, S. Ryu, Anomalous lattice vibrations of single- and few-layer MoS_2. ACS Nano **4**(5), 2695–2700 (2010). doi:10.1021/nn1003937

40. B. Windom, W.G. Sawyer, D. Hahn, A Raman spectroscopic study of MoS_2 and MoO_3: applications to tribological systems. Tribol. Lett. **42**(3), 301–310 (2011). doi:10.1007/s11249-011-9774-x

41. H. Li, Q. Zhang, C.C.R. Yap, B.K. Tay, T.H.T. Edwin, A. Olivier, D. Baillargeat, From bulk to monolayer MoS_2: evolution of Raman scattering. Adv. Funct. Mater. **22**(7), 1385–1390 (2012). doi:10.1002/adfm.201102111

42. L. Kumari, Y.-R. Ma, C.-C. Tsai, Y.-W. Lin, S.Y. Wu, K.-W. Cheng, Y. Liou, X-ray diffraction and Raman scattering studies on large-area array and nanobranched structure of 1D MoO_2 nanorods. Nanotechnology **18**(11), 115717 (2007). doi:10.1088/0957-4484/18/11/115717

43. M.M. Perera, M.-W. Lin, H.-J. Chuang, B.P. Chamlagain, C. Wang, X. Tan, M.M.-C. Cheng, D. Tománek, Z. Zhou, Improved carrier mobility in few-layer MoS_2 field-effect transistors with ionic-liquid gating. ACS Nano **7**(5), 4449–4458 (2013). doi:10.1021/nn401053g

44. B. Chakraborty, A. Bera, D.V.S. Muthu, S. Bhowmick, U.V. Waghmare, A.K. Sood, Symmetry-dependent phonon renormalization in monolayer MoS_2 transistor. Phys. Rev. B **85**(16), 161403 (2012). doi:10.1103/PhysRevB.85.161403

45. M. Buscema, G. Steele, H.J. van der Zant, A. Castellanos-Gomez, The effect of the substrate on the Raman and photoluminescence emission of single-layer MoS_2. Nano Res. **7**(4), 561–571 (2014). doi:10.1007/s12274-014-0424-0

46. X.X. Wei, Y. Cheng, D. Huo, Y.H. Zhang, J.Z. Wang, Y. Hu, Y. Shi, PL enhancement of MoS_2 by Au nanoparticles. Acta Phys. Sin. **63**(21), 217802 (2014). doi:10.7498/aps.63.217802

47. A. Splendiani, L. Sun, Y. Zhang, T. Li, J. Kim, C.-Y. Chim, G. Galli, F. Wang, Emerging photoluminescence in monolayer MoS_2. Nano Lett. **10**(4), 1271–1275 (2010). doi:10.1021/nl903868w

48. L.-P. Feng, J. Su, D.-P. Li, Z.-T. Liu, Tuning the electronic properties of Ti–MoS_2 contacts through introducing vacancies in monolayer MoS_2. Phys. Chem. Chem. Phys. **17**(10), 6700–6704 (2015). doi:10.1039/C5CP00008D

49. C. Ataca, S. Ciraci, Dissociation of H_2O at the vacancies of single-layer MoS_2. Phys. Rev. B **85**(19), 195410 (2012). doi:10.1103/PhysRevB.85.195410

50. D. Liu, Y. Guo, L. Fang, J. Robertson, Sulfur vacancies in monolayer MoS_2 and its electrical contacts. Appl. Phys. Lett. **103**(18), 183113 (2013). doi:10.1063/1.4824893

51. W. Zhou, X. Zou, S. Najmaei, Z. Liu, Y. Shi, J. Kong, J. Lou, P.M. Ajayan, B.I. Yakobson, J.-C. Idrobo, Intrinsic structural defects in monolayer molybdenum disulfide. Nano Lett. **13**(6), 2615–2622 (2013). doi:10.1021/nl4007479

52. S. Bertolazzi, D. Krasnozhon, A. Kis, Nonvolatile memory cells based on MoS_2/graphene heterostructures. ACS Nano **7**(4), 3246–3252 (2013). doi:10.1021/nn3059136

53. Z. Yin, H. Li, H. Li, L. Jiang, Y. Shi, Y. Sun, G. Lu, Q. Zhang, X. Chen, H. Zhang, Single-layer MoS_2 phototransistors. ACS Nano **6**(1), 74–80 (2011). doi:10.1021/nn2024557

54. K. Kalantar-Zadeh, J. Tang, M. Wang, K.L. Wang, A. Shailos et al., Synthesis of nanometre-thick MoO_3 sheets. Nanoscale **2**(3), 429–433 (2010). doi:10.1039/B9NR00320G

55. J.V. Silveira, L.L. Vieira, A.J. Sampaio, O.L. Alves, A.G. Souza Filho, Temperature-dependent Raman spectroscopy study in MoO_3 nanoribbons. J. Raman Spectrosc. **43**(10), 1407–1412 (2012). doi:10.1002/jrs.4058

56. Q. Ji, Y. Zhang, Y. Zhang, Z. Liu, Chemical vapour deposition of group-VIB metal dichalcogenide monolayers: engineered substrates from amorphous to single crystalline. Chem. Soc. Rev. **44**, 2587–2602 (2015). **Advance Article**

57. J. Guo, X. Chen, S. Jin, M. Zhang, C. Liang, Synthesis of graphene-like MoS_2 nanowall/graphene nanosheet hybrid materials with high lithium storage performance. Catal. Today **246**, 165–171 (2015). doi:10.1016/j.cattod.2014.09.028

58. S. Najmaei, Z. Liu, W. Zhou, X. Zou, G. Shi, S. Lei, B.I. Yakobson, J.-C. Idrobo, P.M. Ajayan, J. Lou, Vapour phase growth and grain boundary structure of molybdenum disulphide atomic layers. Nat. Mater. **12**(8), 754–759 (2013). doi:10.1038/nmat3673

59. B. Li, S. Yang, N. Huo, Y. Li, J. Yang, R. Li, C. Fan, F. Lu, Growth of large area few-layer or monolayer MoS_2 from controllable MoO_3 nanowire nuclei. RSC Adv. **4**(50), 26407–26412 (2014). doi:10.1039/c4ra01632g

60. J.M. Soon, K.P. Loh, Electrochemical double-layer capacitance of MoS_2 nanowall films. Electrochem. Solid-State Lett. **10**(11), A250–A254 (2007). doi:10.1149/1.2778851

61. Z. Fan, J. Chen, B. Zhang, B. Liu, X. Zhong, Y. Kuang, High dispersion of γ-MnO_2 on well-aligned carbon nanotube arrays and its application in supercapacitors. Diam. Relat. Mater. **17**(11), 1943–1948 (2008). doi:10.1016/j.diamond.2008.04.015

62. A. Sharma, A. Nayak, R. Ghosh, H.-Y. Chang, The Optoelectronic Properties of CVD Grown MoS_2 Nanowalls. in *NCUR 2014*, University of Kentucky, Lexington, 3–5 April 2014

63. U.K. Sen, S. Mitra, High-rate and high-energy-density lithium-ion battery anode containing 2D MoS_2 nanowall and cellulose binder. ACS Appl. Mater. Interf. **5**(4), 1240–1247 (2013). doi:10.1021/am3022015

64. M.A. Camacho-López, L. Escobar-Alarcón, M. Picquart, R. Arroyo, G. Córdoba, E. Haro-Poniatowski, Micro-Raman study of the m-MoO_2 to α-MoO_3 transformation induced by CW-laser irradiation. Opt. Mater. **33**(3), 480–484 (2011). doi:10.1016/j.optmat.2010.10.028

65. T. Siciliano, A. Tepore, E. Filippo, G. Micocci, M. Tepore, Characteristics of molybdenum trioxide nanobelts prepared by thermal evaporation technique. Mater. Chem. Phys. **114**(2), 687–691 (2009). doi:10.1016/j.matchemphys.2008.10.018